# *Drivers of the ECMWF SEAS5 seasonal forecast for the hot and dry European summer of 2022*

Received: 24 January 2024 | Revised: 28 June 2024 | Accepted: 8 August 2024

DOI: 10.1002/qj.4851

Quarterly Journal of the Royal Meteorological Society RMetS

RESEARCH ARTICLE

# Drivers of the ECMWF SEAS5 seasonal forecast for the hot and dry European summer of 2022

**Matthew Patterson**[1] | **Daniel J. Befort**[2] | **Christopher H. O'Reilly**[1] | **Antje Weisheimer**[3,4]

[1]Department of Meteorology, University of Reading, Reading, UK

[2]European Centre for Medium-Range Weather Forecasts (ECMWF), Bonn, Germany

[3]European Centre for Medium-Range Weather Forecasts (ECMWF), Reading, UK

[4]National Centre for Atmospheric Science (NCAS), University of Oxford, Oxford, UK

**Correspondence**
Matthew Patterson, Department of Meteorology, University of Reading, Whiteknights Road, Earley Gate, Reading, RG6 6ET, UK.
Email: m.r.patterson@reading.ac.uk

**Funding information**
Royal Society University Research Fellowship, Grant/Award Number: URF\R1\201230; European Union Horizon Europe Research and Innovation Programme, Grant/Award Number: 101081460; NERC, Grant/Award Number: NE/V001787/1; NERC, Grant/Award Number: NE/T013451/1

## Abstract

The European summer (June–August) 2022 was characterised by warm and dry anomalies across much of the continent, likely influenced by a northward-shifted jet stream. These general features were well predicted by European Centre for Medium-Range Weather Forecasts' system 5 seasonal forecast, initialised on May 1. Such successful predictions for European summers are relatively uncommon, particularly for atmospheric circulation. In this study, a set of hindcast experiments is employed to investigate the role that initialisation of the ocean, atmosphere, and land surface played in the 2022 forecast. We find that the trend from external forcing was the strongest contributor to the forecast near-surface temperature anomalies, with atmospheric circulation and land-surface interactions playing a secondary role. On the other hand, atmospheric circulation made a strong contribution to precipitation anomalies. Modelled Euro-Atlantic circulation anomalies in 2022 were consistent with a La Niña-forced teleconnection from the tropical Pacific. However, a northward jet trend in the model hindcasts with increasing greenhouse gas concentrations also contributed to the predicted circulation anomalies in 2022. In contrast, the observed linear trend in the jet over the past four decades was a southward shift, though it is unclear whether this trend was driven by external forcings or natural variability. Nevertheless, this case study demonstrates that important features of at least some European summers are predictable at the seasonal time-scale.

**KEYWORDS**

atmospheric circulation, climate modelling, Europe, seasonal prediction, summer

## 1 | INTRODUCTION

The 2022 European summer was the hottest in the European Centre for Medium-Range Weather Forecasts (ECMWF) Reanalysis v. 5 (ERA5) record (Figure 1a; Copernicus, 2022), with a new national temperature record set in the United Kingdom (Zachariah *et al.*, 2022) and heat-related deaths across Europe estimated at 61,672 (Ballester *et al.*, 2023). Many countries, particularly in the Mediterranean region, experienced meteorological (Figure 1b) and hydrological drought (e.g., Bonaldo *et al.*, 2022; Faranda *et al.*, 2023), resulting in the second lowest river discharge across Europe in the Copernicus Emergency Management Service model dataset, which begins in 1991 (Copernicus, 2022). The hot and dry conditions contributed to widespread wildfires, particularly

across Spain, Portugal, and France (Rodrigues *et al.*, 2023). Both warmer temperatures from anthropogenic climate change and the anticyclonic atmospheric circulation across Europe contributed strongly to the summer 2022 weather (Faranda *et al.*, 2023; Ibebuchi & Abu, 2023; Schumacher *et al.*, 2022).

Europe has previously been identified as a particular hotspot for increasing heatwave occurrence and intensity under climate change (Rousi *et al.*, 2022), with recent decades seeing an intensification of heat extremes in the region (Christidis *et al.*, 2015; Patterson, 2023; Perkins-Kirkpatrick & Lewis, 2020). The high societal impact of these increasing extreme events demands for accurate prediction systems for European summer weather and climate.

Current seasonal forecasting systems have shown relatively little skill in predicting atmospheric circulation variability in boreal summer for the European region (Dunstone *et al.*, 2023b; Lockwood *et al.*, 2023; Patterson *et al.*, 2022). This is in contrast to the European winter when forecast systems have shown significant skill in predicting the North Atlantic Oscillation, the leading mode of atmospheric circulation (Athanasiadis *et al.*, 2017; Scaife *et al.*, 2014). This seasonal contrast in skill may partly be due to the relatively weak signals coming from El Niño Southern Oscillation and the stratosphere in comparison with the winter (Domeisen *et al.*, 2015), as well as the smaller spatial scale of typical weather phenomena in summer. Nevertheless, a growing body of literature has suggested that there is potential for predictability of summer Euro-Atlantic circulation on seasonal time-scales. For instance, recent observational studies have found that the summer East Atlantic pattern is modulated by forcing from tropical convection (O'Reilly *et al.*, 2018; Rieke *et al.*, 2021; Wulff *et al.*, 2017), while North Atlantic sea-surface temperatures (SSTs) also affect circulation over the Euro-Atlantic (Beobide-Arsuaga *et al.*, 2023; Osborne *et al.*, 2020; Ossó *et al.*, 2018, 2020). Moreover, recent work has suggested that the summer North Atlantic Oscillation may be partly predictable via the date of the stratospheric vortex breakdown (Dunstone *et al.*, 2023b; Wang & Ting, 2022).

Regarding other variables, Dunstone *et al.* (2018) showed moderate skill for European rainfall in the UK Met Office model, which they attributed largely to the effect of North Atlantic SSTs on atmospheric moisture availability. Initialisation of the land surface also appears to provide some predictability via soil moisture feedbacks with the atmosphere (Ardilouze *et al.*, 2017; Prodhomme *et al.*, 2016; Seneviratne *et al.*, 2010), particularly on subseasonal time-scales (Orth & Seneviratne, 2014). Furthermore, the study of Patterson *et al.* (2022) identified the significant role that external forcing from greenhouse gases and aerosols has on seasonal predictions of 2-m temperature (T2m), with models deriving much of their T2m skill over Europe from the forced trend.

In the context of relatively low European summer forecast skill, it is interesting that many large-scale characteristics of the 2022 summer were relatively well forecast for Europe by ECMWF's system 5 (SEAS5; Johnson *et al.*, 2019). This raises the question of whether atmospheric circulation, temperature, and precipitation were inherently more predictable in summer 2022 than in other years, a problem that we investigate in this study. Moreover, we seek to address the following questions:

- How well did ECMWF's SEAS5 capture the observed circulation and near-surface anomalies in European summer 2022?
- What determined the circulation patterns in observations and the forecast? Did the forecast capture circulation anomalies for the "right reasons"?
- What role did the atmospheric circulation, externally forced trends, and soil moisture anomalies play in driving the forecast near-surface conditions?

The study is structured as follows: data sources, seasonal hindcast experiments, and statistical methods are described in Section 2, and the hindcast is evaluated against observations in Section 3. Following this, the drivers of the circulation anomalies in the forecast and observed anomalies are analysed in Section 4. Next, the roles of atmospheric circulation, soil moisture, and externally forced trends in the forecast anomalies are investigated in Section 5. Finally, a discussion of the results is provided in Section 6.

## 2 | DATA AND METHODS

### 2.1 | Observations and reanalysis datasets

In this work, we use monthly mean data from the ERA5 dataset (Hersbach *et al.*, 2020) for all variables with the exception of precipitation, which is investigated using the monthly mean Global Precipitation Climatology Project (GPCP) version 2.3 (Adler *et al.*, 2018).

### 2.2 | ECMWF's SEAS5

We briefly provide a few details on SEAS5, but refer the interested reader to Johnson *et al.* (2019) for further information. SEAS5 is based on cycle 43r1 of the Integrated Forecast System and consists of coupled atmospheric,

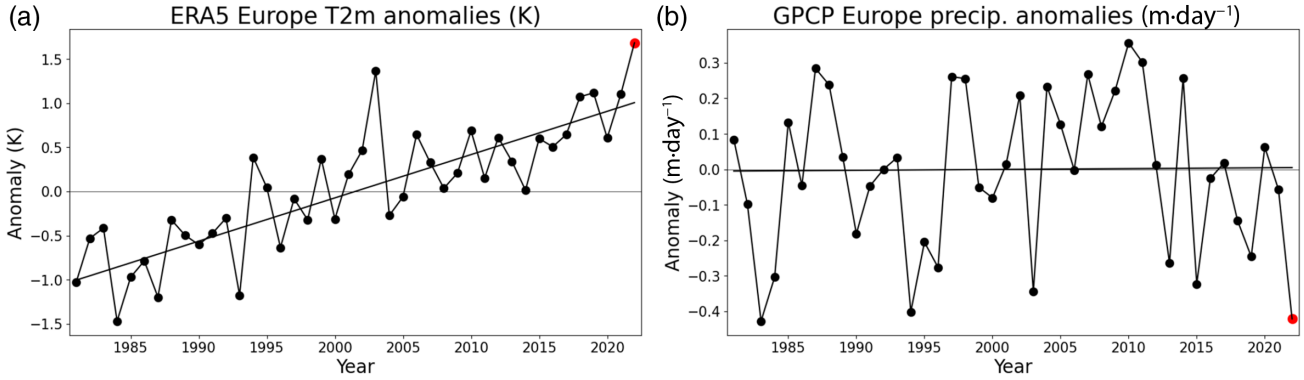


**FIGURE 1** Time series of observed (a) 2-m temperature (T2m; European Centre for Medium-Range Weather Forecasts Reanalysis v. 5, ERA5) and (b) precipitation (Global Precipitation Climatology Project, GPCP) anomalies for European summers (1981–2022), averaged over land 35°N–63°N, 10°W–30°E. Anomalies are calculated relative to 1981–2021. The year 2022 is shown by a red dot, and the linear trend line for the years 1981–2021 is also plotted. [Colour figure can be viewed at wileyonlinelibrary.com]

oceanic, and prognostic sea-ice components. The atmosphere is run at T319 horizontal resolution with 91 levels in the vertical, whereas the ocean is ORCA025 (0.25°) with 75 levels in the vertical. Both the atmosphere and land surface are initialised using ECWMF operational analyses, and the ocean and sea-ice are initialised using OCEAN5 (Zuo *et al.*, 2019), a combination of historical ocean reanalysis (ORAS5) and the daily real-time ocean analysis (OCEAN5-RT). Greenhouse gases are prescribed following the Coupled Model Intercomparison Project phase 5 Representative Concentration Pathway scenario 3-PD, and tropospheric sulfate aerosol follows the decadally varying Coupled Model Intercomparison Project phase 5 climatology.

This study makes use of SEAS5 hindcasts and forecasts of past summers spanning 1981–2016 and 2017–2021 respectively. The set-up for the hindcasts and forecasts is almost identical, and the primary distinction between the two is that the hindcasts are initialised with ERA5 and forecasts are initialised with ECWMF analyses. The years from 2017 are forecasts, as the system became operational in that year. The SEAS5 hindcasts and forecasts each have 51 members for each start date. Throughout this study, anomalies are identified with respect to the period 1981–2021.

## 2.3 | Summer 2022 hindcast experiments

In order to investigate the impacts of initialisation of different components of the forecast system, we perform a number of hindcast experiments using the same set-up of the Integrated Forecast System as used for SEAS5, including the same grid resolutions in the atmosphere and ocean. Each of these simulations is initialised on May 1 and run for 4 months. A hindcast experiment identical to the operational forecast is performed ("CONTROL"), but extended to 200 members rather than 51. In order to clarify the role of ocean initial conditions in driving the forecast, we perform a set of hindcasts with initial conditions for the atmosphere and land surface taken from a year in the range [1981, 2021] but with 2022 ocean initial conditions. This experiment is referred to as "OCEAN-IC-2022." For example, for a particular ensemble member, the ocean initial conditions are taken from 2022 and all other conditions are taken from the year 1990. For each of the 41 years in [1981, 2021], five simulations are run with perturbed ocean initial conditions for 2022 (the operational forecasts also use perturbed ocean initial conditions) making a total of $41 \times 5 = 205$ ensemble members. Similarly, a set of simulations is performed with ocean initial conditions from the years [1981, 2021] but all other conditions taken from 2022 ("ATMOS-IC-2022") to identify the role that other drivers play.

Consequently, some of the effects of external forcing are present in both OCEAN-IC-2022 and ATMOS-IC-2022. That is, OCEAN-IC-2022 is driven by 2022 SSTs, which have warmed with greenhouse gas forcing. On the other hand, the atmosphere in ATMOS-IC-2022 will be warmed as a result of the warmer initial atmospheric state and the presence of 2022 greenhouse gas forcing. The atmosphere and ocean will be out of balance in ATMOS-IC-2022 and OCEAN-IC-2022 as the ocean is warm and the atmosphere cold or vice versa. However, we will show that the results do not appear to be strongly affected by this as the sum of the ensemble-mean anomalies in ATMOS-IC-2022 and OCEAN-IC-2022 is approximately equal to the CONTROL. The experiments are summarised in Table 1.

## 2.4 | Circulation analogues

To identify the impact of atmospheric circulation in the 2022 seasonal hindcasts on T2m and precipitation, we

**TABLE 1** A summary of the hindcast experiments performed in this study, including information on the initialisation.

| Experiment | Members | Ocean | Atmosphere | Land surface | External forcing |
|---|---|---|---|---|---|
| CONTROL | 200 | 2022 conditions | 2022 conditions | 2022 conditions | 2022 conditions |
| OCEAN-IC-2022 | 205 | 2022 conditions | [1981, 2021] | [1981, 2021] | [1981, 2021] |
| ATMOS-IC-2022 | 205 | [1981, 2021] | 2022 conditions | 2022 conditions | 2022 conditions |

*Note*: In this table, [1981, 2021] indicates that initial conditions of each of the ensemble members in these experiments are taken from a random year between 1981 and 2021.

use a circulation analogues method inspired by Jézéquel *et al.* (2018). The method estimates the circulation-related component of other variables by identifying periods with similar atmospheric states and averaging the variable in question over those similar states. There are a few ways in which our methodology differs from Jézéquel *et al.* (2018). First, Jézéquel *et al.* (2018) utilise daily data whereas we use means over June–August (JJA); second, we represent atmospheric circulation anomalies by 500 hPa stream function anomalies ($\psi 500'$) rather than 500 hPa geopotential height anomalies. We make this choice because the latter field is directly affected by temperature changes, such as through global warming, whereas $\psi 500$ only reflects circulation variability.

Our methodology proceeds by first removing the global warming signal from variables in the SEAS5 hindcast/forecast ensemble, spanning 1981–2021, by linearly regressing out the global-mean, ensemble-mean T2m. We then take the JJA-mean $\psi 500'_{2022,i}$ (i.e., the $i$th member from the 2022 SEAS5 CONTROL experiment) and compare with $\psi 500'$ in all ensemble members in the SEAS5 hindcast/forecast ensemble. The most similar $N = 30$ members to the target ($\psi 500'_{2022,i}$) over the Euro-Atlantic region (10°W–30°E, 30°N–80°N) from this 51-member × 41-year = 2091 set are selected. The similarity of the two $\psi 500'$ fields is calculated via area-weighted sums of the absolute values of Euclidian distances between values at each grid point. The average over the $N$ most similar members is then calculated for $\psi 500'$, T2m, and precipitation. However, the magnitudes of the analogue $\psi 500'$ anomalies are typically smaller than the target ($\psi 500'_{2022,i}$) due to being averaged over $N$ members. Hence, we scale the analogue by the ratio of the spatial means of the absolute values over the Euro-Atlantic region for the target relative to the analogue such that the analogues show a similar magnitude to the 2022 anomalies. That is, we scale the analogues by

$$\alpha = \frac{\langle |\psi 500'_{2022,i}| \rangle_{\text{E-A}}}{\langle |(\sum^{N} \psi 500'_{y,j})/N| \rangle_{\text{E-A}}}, \quad (1)$$

where angled brackets represent a spatial average over the Euro-Atlantic region and vertical lines indicate the absolute value. Here, the sum is over the $N$ most similar states with $y$ and $j$ representing the year and member number for those particular states in the hindcast/forecast ensemble respectively. This process is repeated for all 200 CONTROL members and all of these analogues averaged.

## 3 | THE 2022 SUMMER SEASON

First, we analyse the 2022 European season and assess the SEAS5 CONTROL hindcast. Figure 2 compares JJA 2022 anomalies in T2m, precipitation, and 500 hPa zonal wind (U500) and sea-level pressure in observation-based datasets (GPCP for precipitation and ERA5 for other variables) with ensemble-mean anomalies predicted by SEAS5 for forecasts initialised on May 1. Broadly speaking, the CONTROL hindcast qualitatively captures the observed anomalously hot and dry conditions (Figure 2a,b,e,f), though it does not capture the northward and westward extent of the dry anomaly over the United Kingdom. For further context, T2m and precipitation anomalies in SEAS5 hindcasts of past summers are largely positively correlated with observed values over western and central Europe. However, these correlations are not statistically significant (Supporting Information Figures S1 and S2).

With respect to atmospheric circulation, the model, as in observations, features a northward-shifted jet (Figure 2c,g) and positive summer North Atlantic Oscillation pattern, though the positive sea-level pressure anomaly does not extend into Europe in the model (Figure 2h). There is also an easterly wind anomaly, stretching from the Atlantic through to the Mediterranean, which is present in both the forecast model (Figure 2g) and observations (Figure 2c). Note that this easterly wind anomaly is primarily a feature in the mid to lower troposphere and is not present at upper levels (not shown). Interestingly, other seasonal forecast systems within the Copernicus Climate Change archive all predicted an anomalously warm and dry summer (Supporting Information Figures S3 and S4), whereas at least five out of the eight systems predicted a high over the Atlantic,

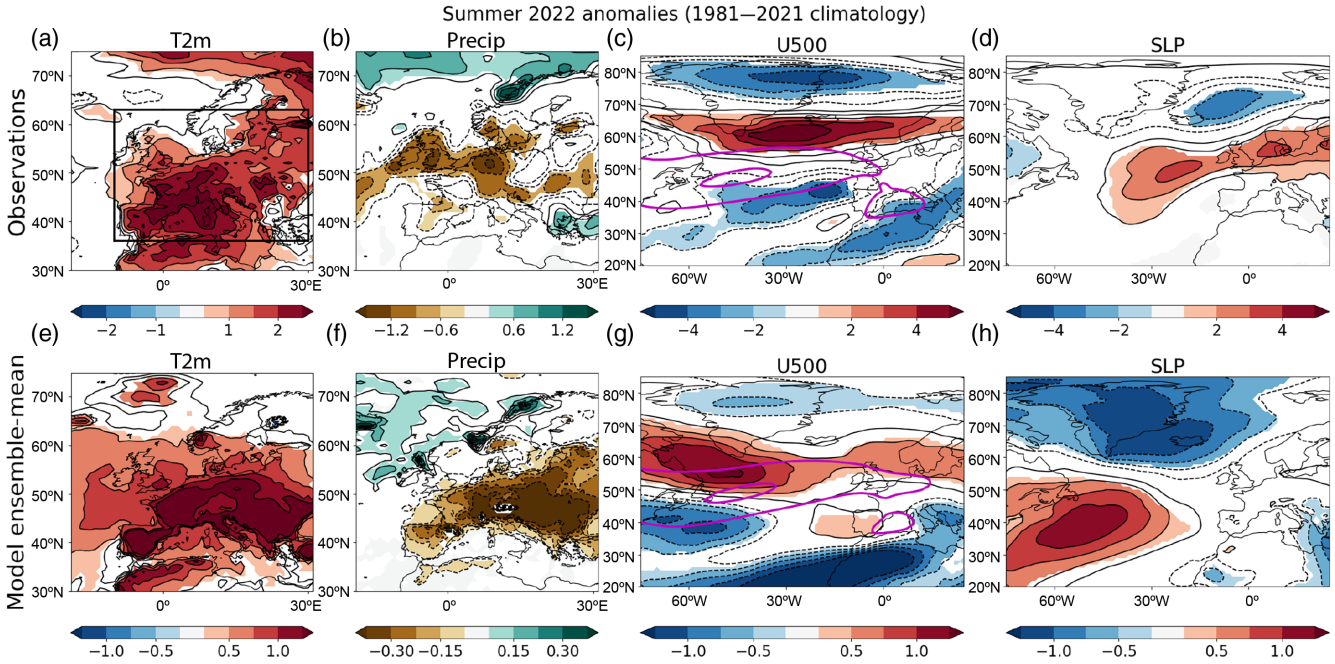


**FIGURE 2** Comparison of (a–d) observed and (e–h) SEAS5 ensemble-mean forecast anomalies for the European summer (June–August, JJA) 2022. The variables shown by colours are (a, e) 2-m temperature (T2m, K), (b, f) precipitation (mm·day$^{-1}$), (c, g) 500 hPa zonal wind (U500; m·s$^{-1}$), and (d, h) sea-level pressure (SLP; hPa). Anomalies are taken with respect to 1981–2021, and anomalies are only coloured for values that exceed one standard deviation from the mean. Values less than a standard deviation from the mean are shown by unfilled contours, with the same contour interval. Note the differing colour scales between the model and observations. In (c) and (g), unfilled, pink contours indicate the 500 hPa zonal wind climatological values for the 10 and 15 m·s$^{-1}$ contours. The box in (a) indicates the European region used in Figures 1 and 3. [Colour figure can be viewed at wileyonlinelibrary.com]

to the southwest of the United Kingdom (Supporting Information Figure S5). This consistency amongst models hints at the presence of a predictable signal in the summer 2022 forecasts.

Next we investigate whether the ensemble can reproduce the magnitude of the observed temperature and precipitation anomalies and attempt to understand the role of atmospheric circulation in driving these anomalies. We calculate the best members at reproducing the patterns of U500, T2m, and precipitation separately by calculating the area-weighted sum of Euclidian distances between observations and each model ensemble member, at each grid point over a specified region, for the given variable. The regions over which the Euclidian distances are calculated are shown by boxes in Figure 3a,e,i. The best member is the member for which the sum of distances is minimised. The northward-shifted jet is best reproduced by member 137, with a similar magnitude of U500 anomalies in this case (Figure 3a). This member also shows a magnitude of T2m and precipitation anomalies similar to the observations (Figure 3b,c vs. Figure 2a,b). The observed patterns of precipitation (Figure 3c) and temperature (Figure 3b) anomalies are largely reproduced in this member, particularly the dry anomalies over northwest Europe (Figure 3c). The region of anomalously low precipitation is notably further north and west in member 137, compared with the ensemble-mean (Figure 3c vs. Figure 2f). This suggests that circulation plays some role in driving these anomalies. However, this member does show enhanced warm and dry anomalies in northeastern Europe (Figure 3b,c), unlike in observations (Figure 2a,b).

The best T2m anomaly pattern (member 164) is similar in total magnitude to ERA5 (Figure 3e,j), as is the best precipitation pattern (member 148) to GPCP (Figure 3i,k). However, the circulation anomalies are quite different for members 148 and 164 (Figure 3d,g) from member 137 (Figure 3a), which has the best U500 pattern. This suggests that temperature and precipitation anomalies in members 148 and 164 (Figure 3e,f,h,i) may arise for slightly different reasons than in member 137. It is worth noting that nearly all ensemble members predicted a warmer than average European summer for 2022 (Figure 3j), which is unsurprising given the strong warming trend (Patterson *et al.*, 2022). The majority of members also predicted a drier than average summer (Figure 3k). This suggests a robust signal in the initial conditions, particularly given that there is no strong trend in European summer precipitation (Figure 1b). Overall, the observed anomalies in precipitation and temperature were well captured by the ensemble.

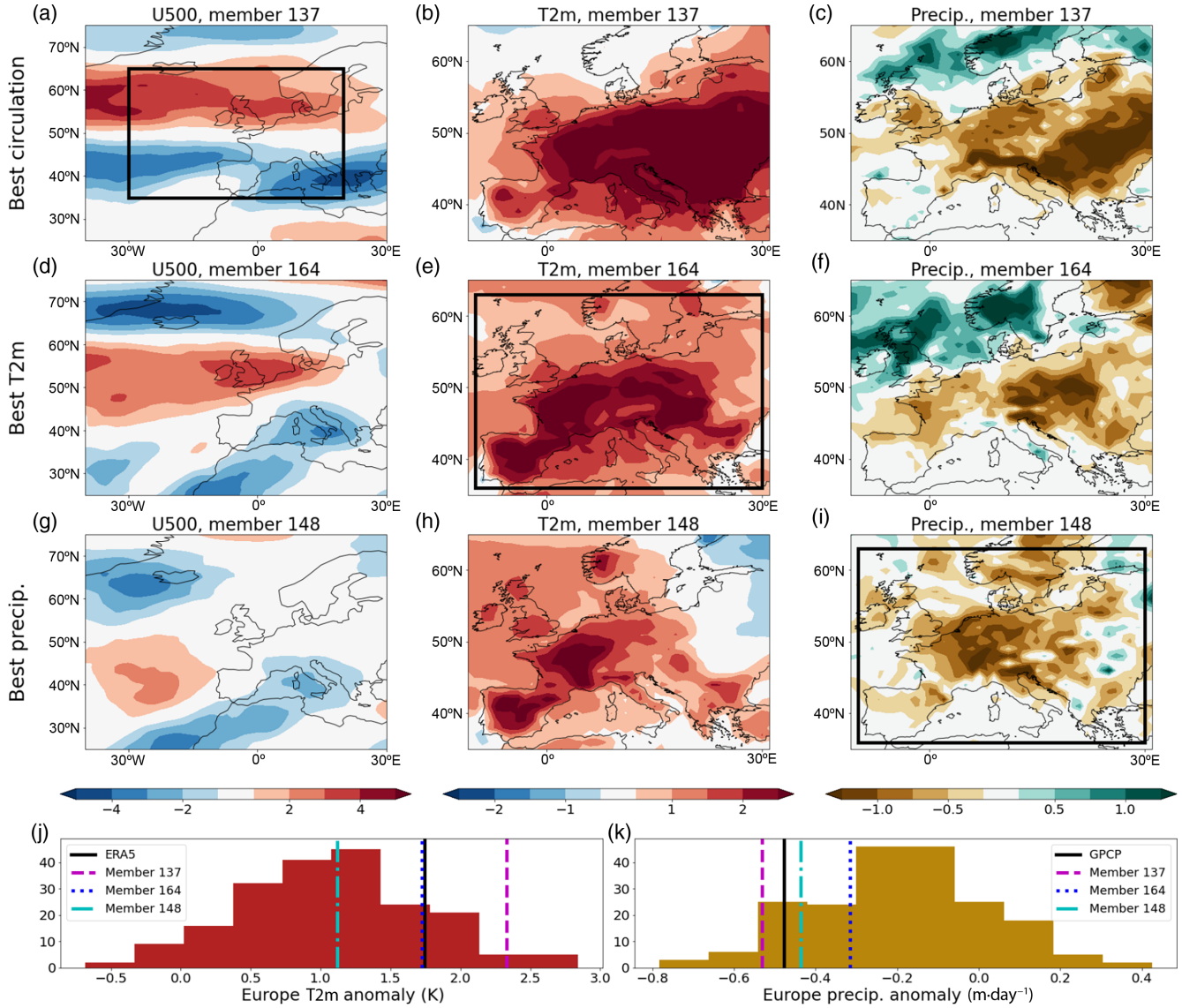


**FIGURE 3** Analysis of individual members within the CONTROL ensemble. The (a) 500 hPa zonal wind (U500), (b) 2-m temperature (T2m), and (c) precipitation anomalies are shown for the member with the most similar pattern over the boxed region with respect to the observed circulation (see text for details). The members with the most similar pattern to observations for (d–f) T2m and (g–i) precipitation are also shown for the same three variables. In (a), (e), and (i), boxes show the region over which the similarity between ensemble members and observations is calculated. Histograms of European-mean (j) T2m and (k) precipitation are also shown, with vertical lines indicating the 2022 values for European Centre for Medium-Range Weather Forecasts Reanalysis v. 5 (ERA5)/Global Precipitation Climatology Project (GPCP) and the best members. [Colour figure can be viewed at wileyonlinelibrary.com]

## 4 | POTENTIAL DRIVERS OF THE OBSERVED AND FORECAST CIRCULATION

In this section we examine the conditions prior to summer 2022 and investigate potential large-scale drivers of European summer weather in that season. At the start of May, the tropical Pacific was characterised by cool SST anomalies, the last of three consecutive La Niña years (Figure 4a). O'Reilly *et al.* (2018) found that La Niña events are typically associated with anticyclonic conditions over the North Atlantic and observed 2022 circulation anomalies were consistent with this (Figure 2c,d). Furthermore, there is some evidence of an anomalous wave train from the Pacific towards the North Atlantic in summer 2022 (Supporting Information Figure S6). SSTs around the United Kingdom and western Europe were also slightly warmer than average (Figure 4a). It is possible that this could have warmed western Europe to some extent via advection of warmer near-surface air or by generating atmospheric circulation anomalies. Following a drier than average spring, soil moisture levels were low at the beginning of May,

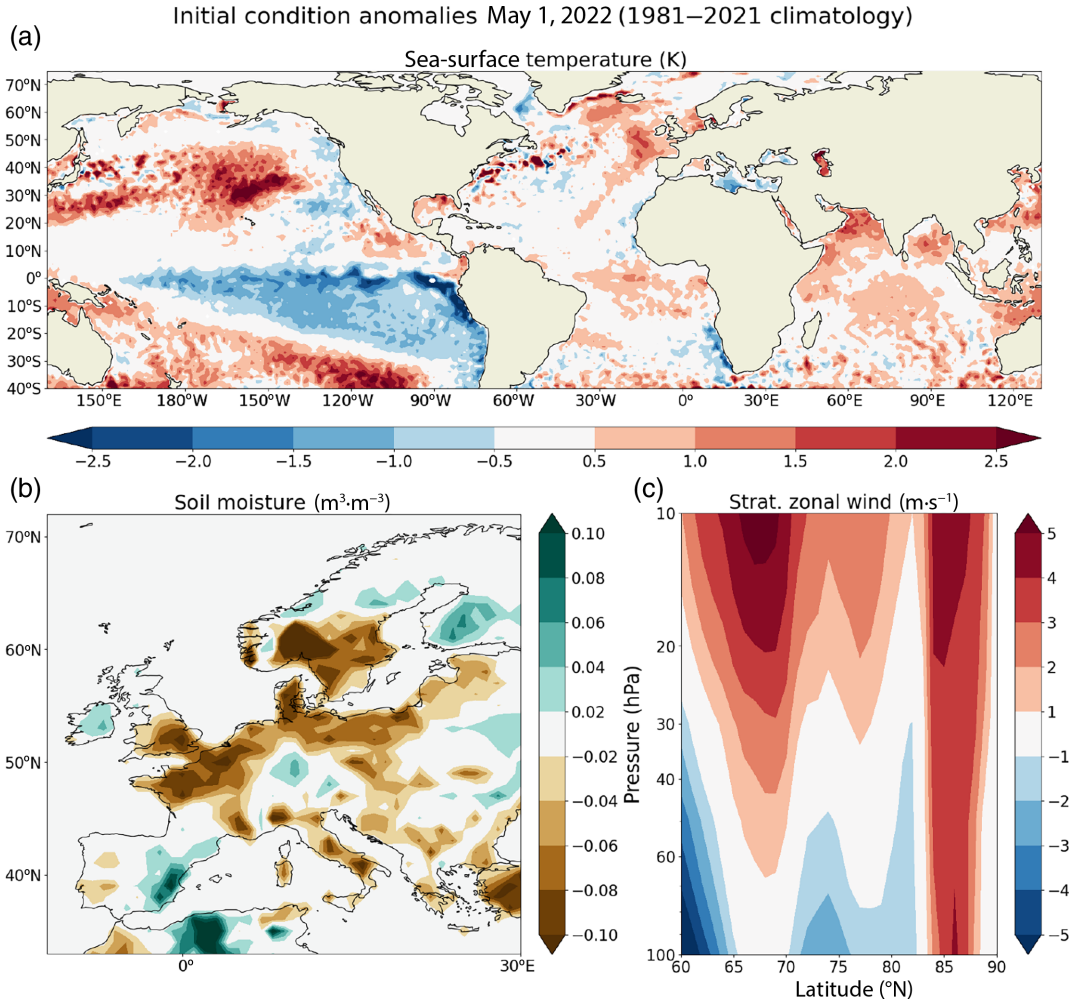


**FIGURE 4** Anomalies for the May 1, 2022, are shown for (a) sea-surface temperatures, (b) soil moisture, and (c) zonal-mean zonal wind in the lower to mid stratosphere. Anomalies are calculated with respect to the April–May mean 1981–2021. [Colour figure can be viewed at wileyonlinelibrary.com]

particularly in northern parts of Europe (Figure 4b). Interestingly, the May soil moisture anomaly pattern resembles the 2022 JJA-mean precipitation anomaly pattern (Figures 4b and 2b). Wang and Ting (2022) and Dunstone *et al.* (2023b) found that positive summer North Atlantic Oscillation years were proceeded by a strong polar vortex in May; hence, we also include stratospheric zonal wind anomalies in Figure 4c. The vortex strength, defined following Dunstone *et al.* (2023b) as the standardised 50 hPa zonal-mean zonal wind anomaly averaged 60°N–80°N, was slightly stronger than average at +0.8 standard deviations above the mean.

In this section, we attempt to attribute the observed 2022 atmospheric circulation anomalies to forcing from various drivers, including Niño 3.4 SSTs, the stratospheric vortex strength, and circulation trends, using a multiple regression framework. Note that there are likely to be other drivers for the observed 2022 North Atlantic circulation, and we later discuss some other possible drivers. The linear trend is included as a predictor because of the substantial southward jet trend seen in this region in summer (Harvey *et al.*, 2023). The drivers of this trend are unclear, though these may include external forcing by aerosols or greenhouse gases, or internal climate variability (Dong & Sutton, 2021). Monthly mean ERA5 data 1981–2021 are used to create the multiple regression model. The SST in the Niño 3.4 region (i.e., 170°W–120°W, 5°S–5°N) is used as a predictor with the JJA mean used to capture any contemporaneous driving of the North Atlantic circulation; for example, via a Rossby wave train. A May polar vortex index is defined again following the method of Dunstone *et al.* (2023b), as described earlier herein. The trend index is simply an index that increases linearly with time between 1981 and 2021. The regression maps are then multiplied by the predictor values in 2022 to gauge the potential influence of these predictors on the observed circulation.

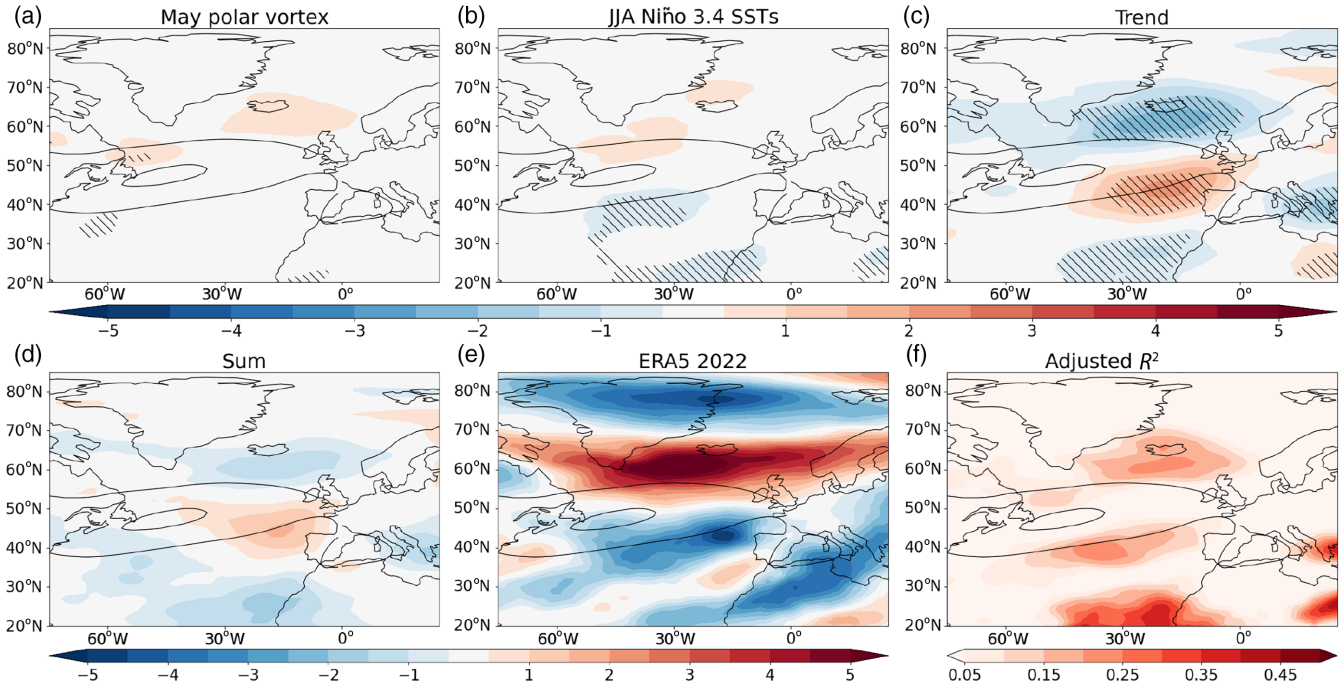


**FIGURE 5** Drivers of 2022 500 hPa zonal wind (U500) in European Centre for Medium-Range Weather Forecasts Reanalysis v. 5 (ERA5) calculated via a multiple linear-regression analysis of past U500 variability (1981–2021) with several predictor variables (see text for details). For each regression map, the coefficients have been multiplied by the 2022 value for the corresponding predictor to indicate the potential impact of that predictor on 2022 U500. The predictors are (a) May 50 hPa zonal wind anomalies (60°N–80°N), (b) June–August (JJA) Niño 3.4 sea-surface temperatures (SSTs), and (c) the linear trend in JJA U500. Also shown are (d) the sum of the regression coefficients multiplied by the 2022 values and (e) the actual 2022 anomalies. (f) The adjusted $R^2$ values for the multiple regression model. Hatching in (a)–(c) indicates where regression coefficients have $P$ values less than 0.05 following a Student's $t$ test. Note that these $P$ values are calculated for the regression coefficients and not for the product of the coefficients and 2022 predictor value. Units for (a)–(e) are $m \cdot s^{-1}$. The ERA5 JJA U500 climatology is shown in all panels by unfilled contours, with only contours 10 and 15 $m \cdot s^{-1}$ drawn. [Colour figure can be viewed at wileyonlinelibrary.com]

Applying the multiple-regression framework to observed circulation over the past 41 years suggests that the linear trend dominates the predicted 2022 U500 anomalies over predicted U500 anomalies from Niño 3.4 SSTs and the May vortex strength (Figure 5a–c). Positive May polar vortex anomalies may have contributed to a slight northward shift of the jet at the jet exit (i.e., the region where the jet weakens substantially; Figure 5a), and cool tropical Pacific SSTs may have also shifted the western portion of the jet further north and generated easterly anomalies in the subtropical North Atlantic (Figure 5b). However, the magnitude of the predicted U500 anomalies from the linear trend is larger than from either of these two other predictors and is instead characterised by a southward shift of the jet (Figure 5c).

This statistical model therefore cannot predict the observed northward shift (Figure 5d,e). On the other hand, predicted easterly anomalies in the Mediterranean and over North Africa show some similarity with the observed 2022 circulation (Figure 5d,e). With that said, overall the 2022 circulation was not attributable on the basis of these three drivers alone. This may not be too surprising given that predictable drivers can only explain a proportion of the observed circulation as a significant proportion of the observed circulation will arise from random, unforced variability, particularly in summer (Franzke & Woollings, 2011). To quantify the proportion of U500 variability that is explained by the regression model, we plot the adjusted $R^2$ statistic, $\overline{R^2}$, defined as

$$\overline{R^2} = 1 - (1 - R^2)\frac{n-1}{n-p-1}. \quad (2)$$

Here, $R$ is the correlation between the regression model prediction and the actual circulation over the historical period, $n = 41$ is the number of years, and $p = 3$ is the number of explanatory variables. $\overline{R^2}$ therefore accounts for the fact that adding more predictors increases the variance explained due to overfitting. $\overline{R^2}$ reaches values of 0.2–0.25 near Iceland (i.e., it explains 20–25% of the variance; Figure 5f). The regression model therefore only explains a small portion of the historical U500 variability. It is also possible that other drivers could contribute to the circulation variability. Caribbean precipitation (Rieke *et al.*, 2021; Wulff *et al.*, 2017) has been

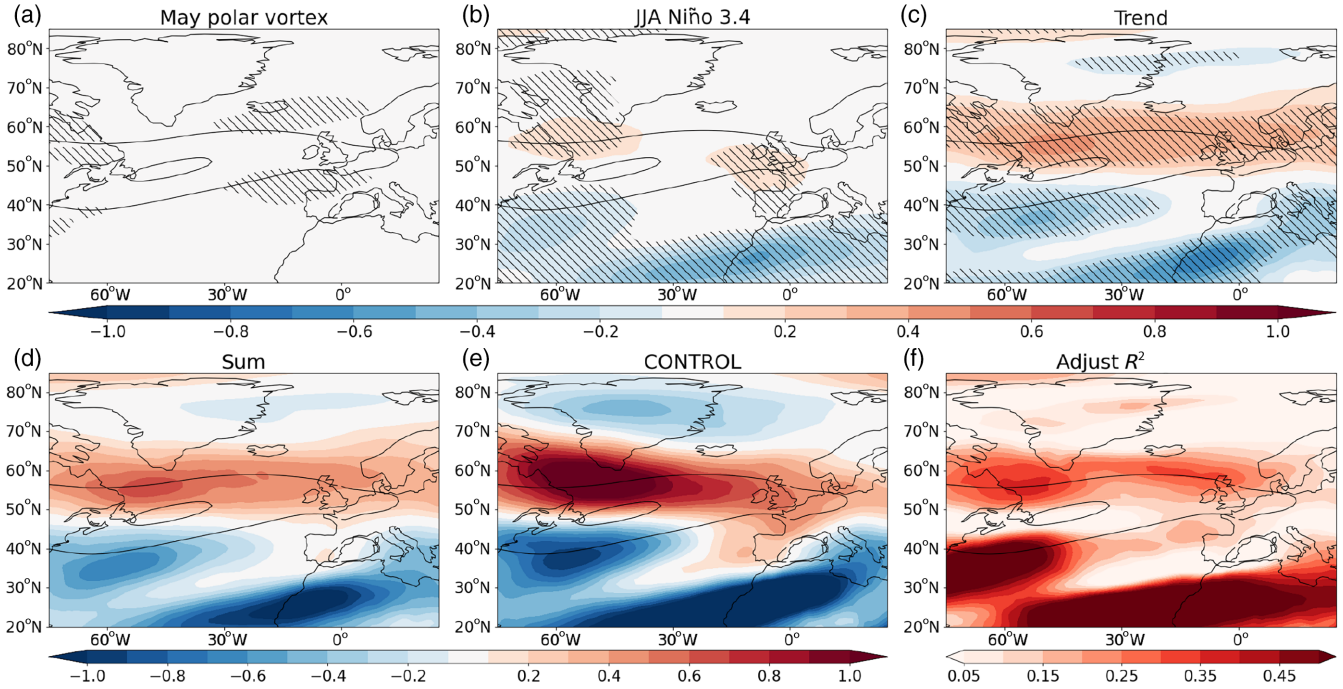


**FIGURE 6** Drivers of CONTROL 2022 500 hPa zonal wind (U500) calculated via a multiple linear-regression analysis of ensemble-mean U500 variability from SEAS5 hindcasts/forecasts (1981–2021) with several predictor variables (see text for details). This uses the same method as in Figure 5, but using the SEAS5 hindcast/forecast ensemble means (1981–2021) for each year to construct the multiple regression and multiplying these by the 2022 CONTROL predictor values. Panel descriptions are the same as for Figure 5. The SEAS5 June–August (JJA) U500 climatology is shown in all panels by unfilled contours, with only contours 10 and 15 $m \cdot s^{-1}$ drawn. [Colour figure can be viewed at wileyonlinelibrary.com]

suggested as a potential driver of summer atmospheric circulation, though using the Pacific–Caribbean dipole index of Wulff *et al.* (2017) as a predictor has little impact on the multiple regression model (Supporting Information Figure S7). North Atlantic SSTs are a further possible driver (Beobide-Arsuaga *et al.*, 2023; Dunstone *et al.*, 2019; Osborne *et al.*, 2020; Ossó *et al.*, 2018, 2020). The initial SST conditions in this region do not appear to map strongly onto the driving patterns in Ossó *et al.* (2018) or the tripole pattern of Dunstone *et al.* (2018) (Figure 4a). Furthermore, the Dunstone *et al.* (2019) tripole index does not contribute skill to the multiple regression model for 2022 when added as an extra predictor (Supporting Information Figure S8). On the other hand, it is possible that the North Atlantic SST anomalies contributed to the observed circulation pattern in ways not captured by this index.

Given this analysis of observed data, it appears likely that either another driver not considered here was important for the observed jet anomaly or the model correctly predicted the pattern of the observed circulation anomalies for the wrong reasons. Nevertheless, we investigate the drivers of the CONTROL circulation via a similar multiple-regression approach. In this case, we construct the multiple-regression model using the SEAS5 hindcast/forecast ensemble means 1981–2021. Predictors are once again the May vortex strength, JJA Niño 3.4 SST, and JJA U500 trend, all calculated from the model, and we multiply regression maps by the CONTROL ensemble-mean predictor values in Figure 6. Similar to ERA5, the SEAS5 multiple regression suggests that the positive polar vortex anomalies act to push the jet exit northward in the model (Figure 6a). Simultaneously, the Niño 3.4 SSTs shift the jet northward over the western North Atlantic and promote easterly flow over North Africa and the subtropical North Atlantic (Figure 6b).

SEAS5 and ERA5 differ when it comes to the trend, as the SEAS5 hindcast/forecast ensemble shows a northward jet trend (Figure 6c, Supporting Information Figure S9b,d). However, the ERA5 trend arises from a single realisation, whereas the SEAS5 ensemble-mean averages over multiple possible jet time series. To investigate the role of internal climate variability in the jet trend we construct a jet index as the JJA-mean U500 in a northern box (60°W–0°W, 55°N–65°N) minus a southern box (60°W–0°W, 40°N–55°N; see Supporting Information Figure S9a). We then create an ensemble of jet trends by taking a random SEAS5 ensemble member from each year in the hindcast/forecast set, for the years 1981–2021 and calculate the jet trend. We then repeat this 1000 times. Only one of these 1000 synthetic jet trends is more negative than the ERA5 trend (Supporting Information Figure S9c). This suggests that either the model has an insufficient level

of internal variability or does not represent the key driving process of the observed jet trend (or both). On the other hand, the observed trend may be sensitive to the choice of period, as the index appears to become more positive from 2015 onwards, suggesting that internal variability at least plays a role. It is clear that further research is needed to understand the drivers of observed and modelled summer jet trends and low-frequency variability.

The trend signal in SEAS5 is the largest contributor to the ensemble-mean circulation over the signal from the polar vortex and Niño 3.4 SST anomalies (Figure 6a–c). Overall, these three drivers explain the CONTROL anomalies well, with their sum showing a similar pattern and magnitude to those in CONTROL (Figure 6d,e). The SEAS5 multiple-regression model also explains a larger proportion of the variance (Figure 6f) than for ERA5 (Figure 5f). For example, the regression model explains more than 50% of the variance in the Subtropics and up to 25%–30% north of the United Kingdom. This difference is likely because the SEAS5 multiple regression is constructed from ensemble-mean data, thereby filtering out much of the random unforced variability. In the remainder of this article we attempt to further understand the drivers of circulation, near-surface temperature, and precipitation anomalies in CONTROL.

## 5 | HINDCAST EXPERIMENTS

In this section, we examine the hindcast experiments to understand the role that these initial conditions for the ocean, atmosphere, and land surface had in driving the forecast anomalies. We also attempt to account for the temperature and precipitation anomalies in the experiments by considering atmospheric circulation, soil moisture, and externally forced trends.

### 5.1 | Atmospheric circulation

The ATMOS-IC-2022 experiments have the same land surface and atmospheric initial conditions as in 2022 but with ocean initial conditions from random other years, whereas OCEAN-IC-2022 runs have the correct ocean initial state but random atmospheric and land-surface conditions. ATMOS-IC-2022 will contain some of the global warming signal from the presence of 2022 levels of carbon dioxide, but OCEAN-IC-2022 will also show some warming signal relative to the climatology due to the warmer SSTs. Considering atmospheric circulation first, the Euro-Atlantic anomalies in OCEAN-IC-2022 (Figure 7c) are almost identical to the CONTROL hindcast (Figure 7a), both in terms of the northward jet and negative U500 anomalies over the tropical Atlantic and North Africa. In contrast, only a weak anticyclonic feature is present over Europe in ATMOS-IC-2022 (Figure 7b). Nevertheless, this anticyclonic feature may still have an important influence on the temperature and precipitation over Europe. Overall, this suggests that the majority of the circulation signal in CONTROL is derived from anomalous SSTs, but with some circulation features over Europe driven by either atmospheric or land-surface initialisation.

On the other hand, European T2m anomalies are larger in ATMOS-IC-2022 than in OCEAN-IC-2022 (Figure 8b,c), with the pattern in the former matching up closely with CONTROL for Europe (Figure 8a). T2m anomalies in OCEAN-IC-2022 are consistently around 0.2–0.4 K across much of Europe, compared with more than 0.6 K for large parts of Europe in ATMOS-IC-2022. Regarding precipitation, this is more evenly split between the ATMOS-IC-2022 and OCEAN-IC-2022 experiments (Figure 8e,f). Note that anomalies in ATMOS-IC-2022 (Figure 8b,e) and OCEAN-IC-2022 (Figure 8c,f), for both T2m and precipitation, combine approximately linearly to

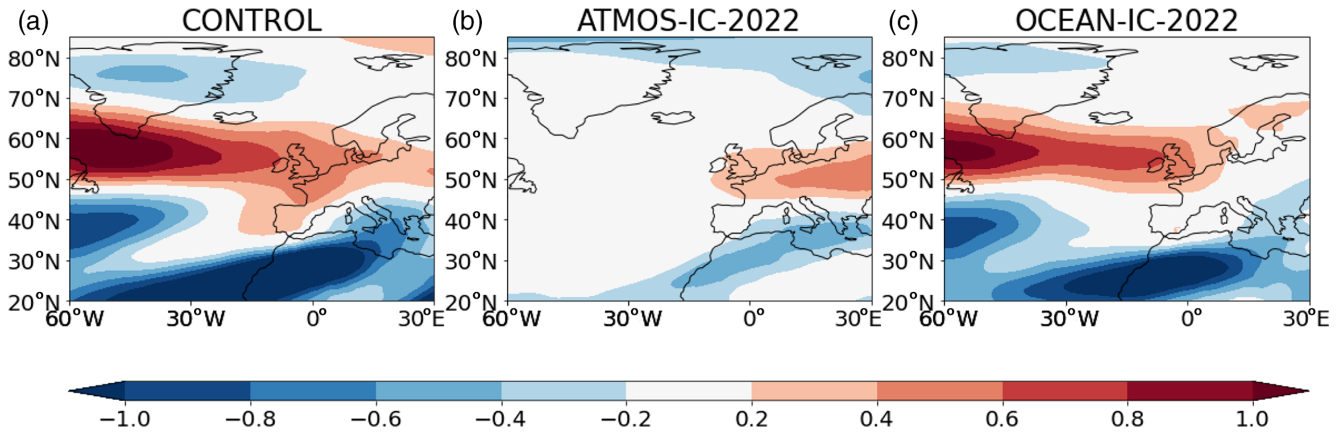


FIGURE 7 June–August-mean 500 hPa zonal wind anomalies in the (a) CONTROL, (b) ATMOS-IC-2022, and (c) OCEAN-IC-2022 experiments. Units are $m \cdot s^{-1}$. [Colour figure can be viewed at wileyonlinelibrary.com]

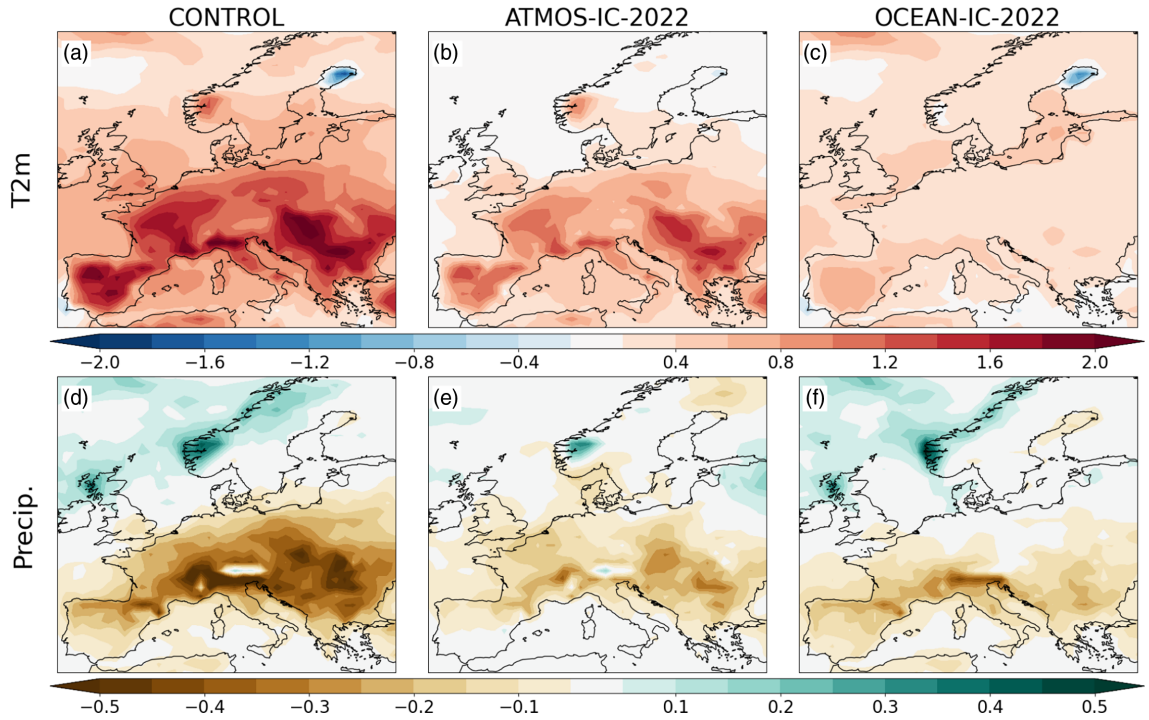


**FIGURE 8** June–August-mean (a–c) 2-m temperature (T2m) and (d–f) precipitation anomalies in the (a, d) CONTROL, (b, e) ATMOS-IC-2022, and (c, f) OCEAN-IC-2022 experiments. Units of T2m and precipitation are K and mm·day$^{-1}$ respectively. [Colour figure can be viewed at wileyonlinelibrary.com]

give the CONTROL anomalies (Figure 8a,d; Supporting Information Figures S10 and S11), suggesting that nonlinear interaction between drivers does not play a substantial role here.

In order to quantify the role that atmospheric circulation plays in the ensemble-mean T2m and precipitation anomalies, we use a circulation analogues method. Briefly, the method compares $\psi 500'$ in each ensemble member in the three experiments with $\psi 500'$ across all members in the SEAS5 hindcast/forecast ensemble (1981–2021). The $N = 30$ hindcast/forecast members most similar to the experiment ensemble member over the Euro-Atlantic region are averaged. Then the magnitude of the circulation analogue is scaled such that it has a similar magnitude to the target $\psi 500'$. Finally, an average is taken over the circulation analogues for each corresponding experiment ensemble member. The method is further detailed in Section 2.4.

The circulation over Europe in all three experiments consists of anomalously anticyclonic flow, particularly over western Europe (Figure 9a–c). Similar to the U500 anomalies (Figure 7), the CONTROL shows the largest $\psi 500'$ (Figure 9a) with ATMOS-IC-2022 showing the weakest circulation anomalies. The $\psi 500'$ circulation analogue patterns capture the main features of these experiments though the centre of the maximum $\psi 500'$ is slightly shifted for the CONTROL and ATMOS-IC-2022 analogues (Figure 9d,e) and stronger for the OCEAN-IC-2022 analogue (Figure 9f). Increasing the number of analogues $N$ to 50 or 100 does not substantially alter the analogue patterns (not shown).

Having established that the circulation analogues can capture the broad features of the experiment circulation anomalies, we examine the temperature and precipitation anomalies corresponding to these analogues. Analogue T2m anomalies for the CONTROL account for 0.2–0.6 K over large parts of western and central Europe (Figure 10a), though this is much smaller than for the CONTROL T2m, which are in excess of 1.2 K over large parts of Europe (Figure 8a) and the residual is large (Figure 10g). In terms of absolute magnitude, the largest circulation contribution to T2m anomalies occurs for the Iberian Peninsula (Figure 8a). Circulation also appears to explain little of the T2m anomalies for the ATMOS-IC-2022 experiment (Figure 10b,h). On the other hand, circulation can account for the majority of the T2m anomalies for OCEAN-IC-2022 over land (Figure 10c,i). It is likely that the T2m anomalies in CONTROL and ATMOS-IC-2022 are primarily driven by the radiative response to higher greenhouse gas levels in 2022, relative to the climatology period.

On the other hand, atmospheric circulation explains a large proportion of the dry precipitation signal in all three experiments (Figure 10d–f). This is particularly true

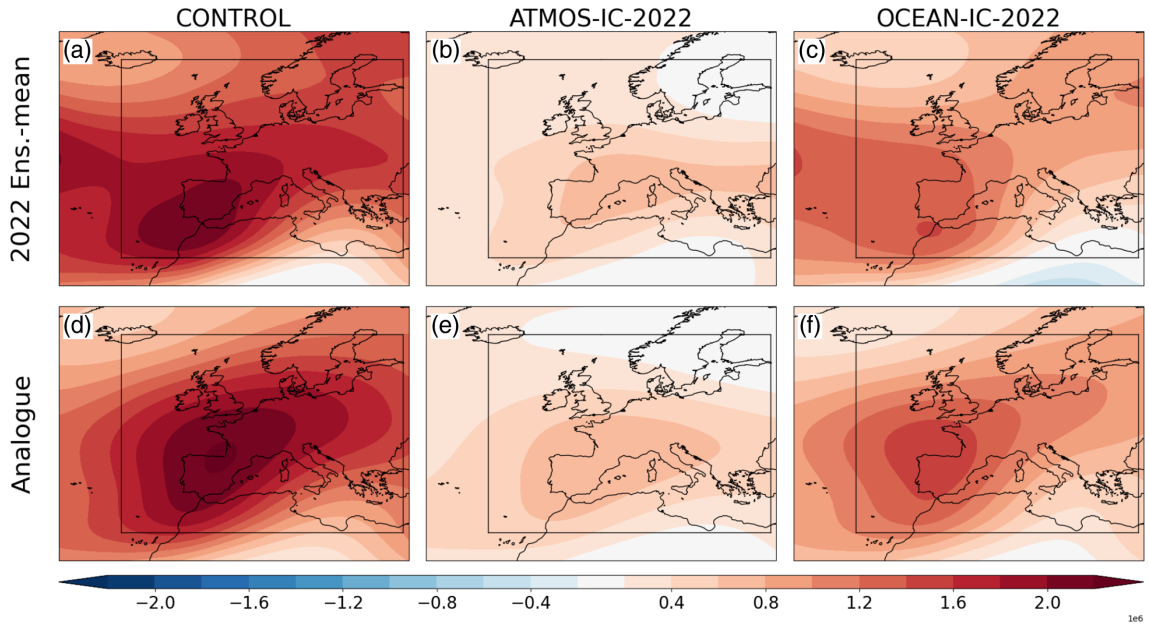


**FIGURE 9** June–August (JJA)-mean, ensemble-mean $\psi 500'$ patterns for each of the three experiments with their corresponding circulation analogues, calculated using the SEAS5 hindcast/forecast ensemble. $\psi 500'$ is shown for (a) CONTROL (b) ATMOS-IC-2022, and (c) OCEAN-IC-2022. Corresponding $\psi 500'$ circulation analogues are shown for the experiments (d) CONTROL, (e) ATMOS-IC-2022, and (f) OCEAN-IC-2022. A box in all panels indicates the Euro-Atlantic region over which the Euclidean distance between hindcast/forecast members and the experiment members is calculated. Units of $\psi 500'$ are $10^6\ s^{-1}$. [Colour figure can be viewed at wileyonlinelibrary.com]

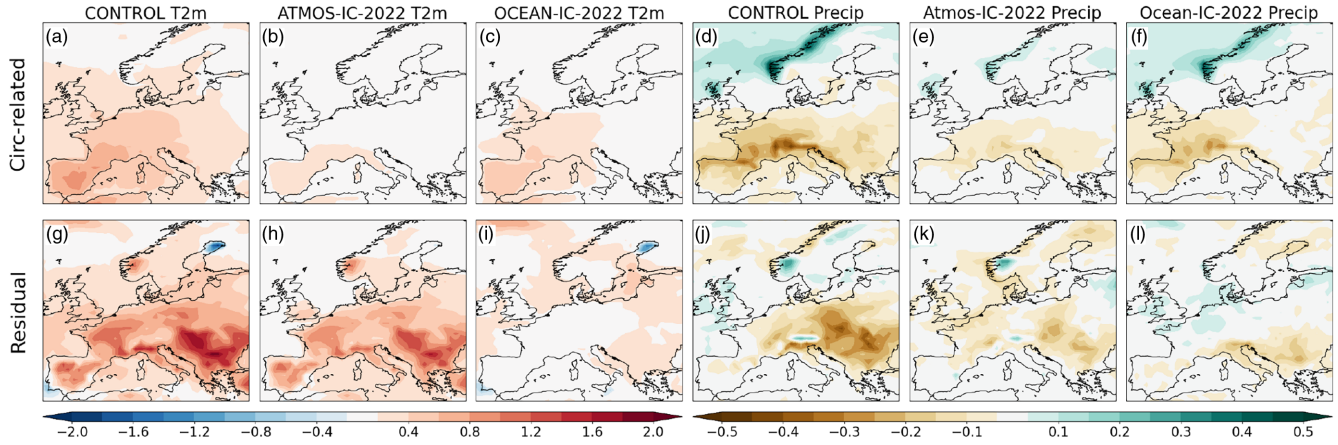


**FIGURE 10** The impact of atmospheric circulation on 2-m temperature (T2m) and precipitation. The circulation analogues' patterns are shown for (a–c) T2m and (d–f) precipitation, for each of the three experiments. The difference between the actual experiment anomalies and the circulation analogue anomalies is shown in (g)–(i) for T2m and (j)–(l) for precipitation. Units of T2m and precipitation are K and $mm \cdot day^{-1}$ respectively. [Colour figure can be viewed at wileyonlinelibrary.com]

for western Europe, where the residuals are smaller than the analogue anomalies (Figure 10d–f compared with Figure 10j–l). The circulation analogues even capture the wet anomalies over the northwest of the United Kingdom and Scandinavian coastline in CONTROL (Figure 10d). The analogues do not capture the magnitude of the dry anomalies over eastern Europe (Figure 10d,j), though it is possible that more localised convection plays a larger role than the large-scale circulation there. We now investigate how other factors, specifically soil moisture and externally forced trends, contribute to the observed T2m and precipitation anomalies.

## 5.2 | Soil moisture

A lack of soil moisture can amplify heat extremes by reducing the amount of cooling from latent heat fluxes.

We investigate the role of soil moisture in shaping the CONTROL forecast using the OCEAN-IC-2022 members, as these have a range of underlying land-surface initial conditions, taken from all years in the range [1981–2021]. Specifically, we calculate a central European soil moisture index for each of the 205 OCEAN-IC-2022 members as the JJA-mean, area-average soil moisture anomaly (48°N–52°N, 0°E–20°E; boxed region in Figure 11a). The global-mean T2m is linearly removed from the index, and other variables are regressed onto this index. The resulting regression maps are then multiplied by the soil moisture index calculated for the CONTROL ensemble-mean to give an indication of how soil moisture may have contributed to the CONTROL T2m and precipitation anomalies. The regression maps therefore show the expected patterns and magnitudes for their respective variables, given the relatively dry conditions in May 2022. The fact that we calculate the soil moisture index using May conditions but regress JJA-mean variables on this index means that the soil moisture deficit is more likely to be causing the changes to the other variables than vice versa.

The results of this analysis are shown in Figure 11. Note that the dry soil moisture anomalies using this index are slightly more widespread across Europe than in the initial conditions, though broadly similar in the overall pattern (Figure 11a compared with Figure 4b). Soil moisture anomalies are associated with weak easterly wind anomalies north of 50°N and a slight dry signal over northern Europe (Figure 11b,d). The dry land surface is also associated with statistically significant positive T2m anomalies (Figure 11c). Soil-moisture-related T2m anomalies account for up to 0.4–0.6 K of the T2m signal in some locations (central to northern Europe, 45°N–60°N, Figure 11c), similar in magnitude to the contribution from atmospheric circulation (Figure 10a). Note that the same contour interval is used for T2m in Figure 11c as in Figures 8a and 10a. Overall, it appears that the dry soil moisture conditions make a substantial contribution to the CONTROL T2m anomalies, particularly in central to northern parts of Europe (Figure 11c).

## 5.3 | Trends and external forcing

Warming trends induced by increased atmospheric carbon dioxide concentration have been shown to be a strong driver of T2m anomalies in seasonal forecasts and provide a large proportion of observed skill (Patterson *et al.*, 2022). We quantify the expected contribution of these trends to surface anomalies by using the combined SEAS5 hindcasts/forecasts ensemble and calculating the JJA-mean trend in the ensemble mean at each grid point, 1981–2021. This trend is then extrapolated to give an expected anomaly in summer 2022. This is shown in Figure 12. The expected T2m anomalies are slightly warmer in southern Europe than in northern Europe, with a magnitude of 0.6–1 K across much of southern and central Europe (Figure 12b). Overall, the trend appears to explain around half the magnitude of the full CONTROL T2m anomalies (Figure 12a,b). Interestingly, precipitation trends in the hindcasts also appear to explain some of the CONTROL signal, particularly a dipole of wet anomalies over northern regions and drying at central latitudes around 45°N–50°N, though overall it is a much lower proportion of the total signal than for T2m (Figure 12b,c,e,f).

Overall, model trends are the strongest contributors to the CONTROL T2m anomalies, with early summer soil moisture and atmospheric circulation playing a

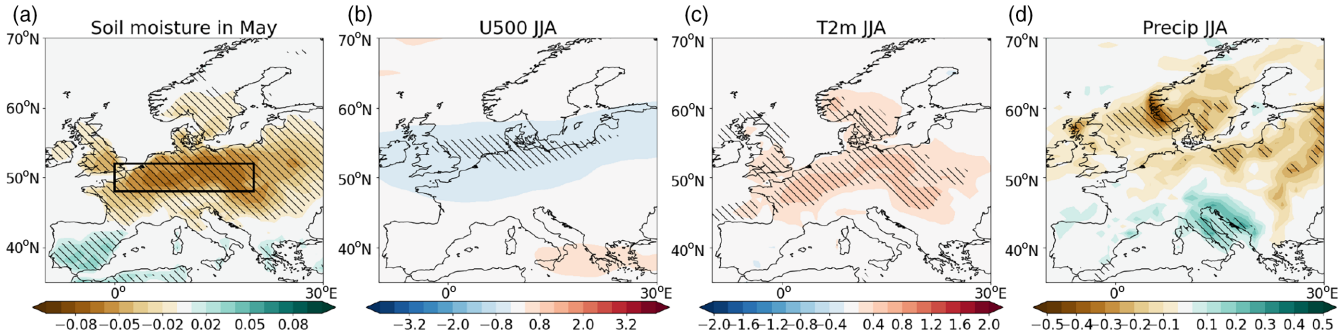


**FIGURE 11** Impact of May soil moisture on different variables in June–August (JJA). The maps show regressions of (a) May soil moisture, (b) JJA 500 hPa zonal wind (U500), (c) JJA 2-m temperature (T2m), and (d) JJA precipitation onto a May soil moisture index, i.e. the May soil moisture averaged in the central European region—box in (a)—in the OCEAN-IC-2022 experiment, but scaled by the mean central European soil moisture in CONTROL. Hence, maps in this figure show the expected pattern and magnitude of each variable, given similar soil moisture conditions to May 2022 in CONTROL. Prior to calculating the regression maps, the global mean T2m signal is also removed from the May soil moisture index. Hatching in all four panels indicates where *P*-values of regression coefficients are less than 0.05, following a Student's *t* test with the null hypothesis of a slope of zero. Units are (a) $m^3 \cdot m^{-3}$, (b) $m \cdot s^{-1}$, (c) K, (d) $mm \cdot day^{-1}$. [Colour figure can be viewed at wileyonlinelibrary.com]

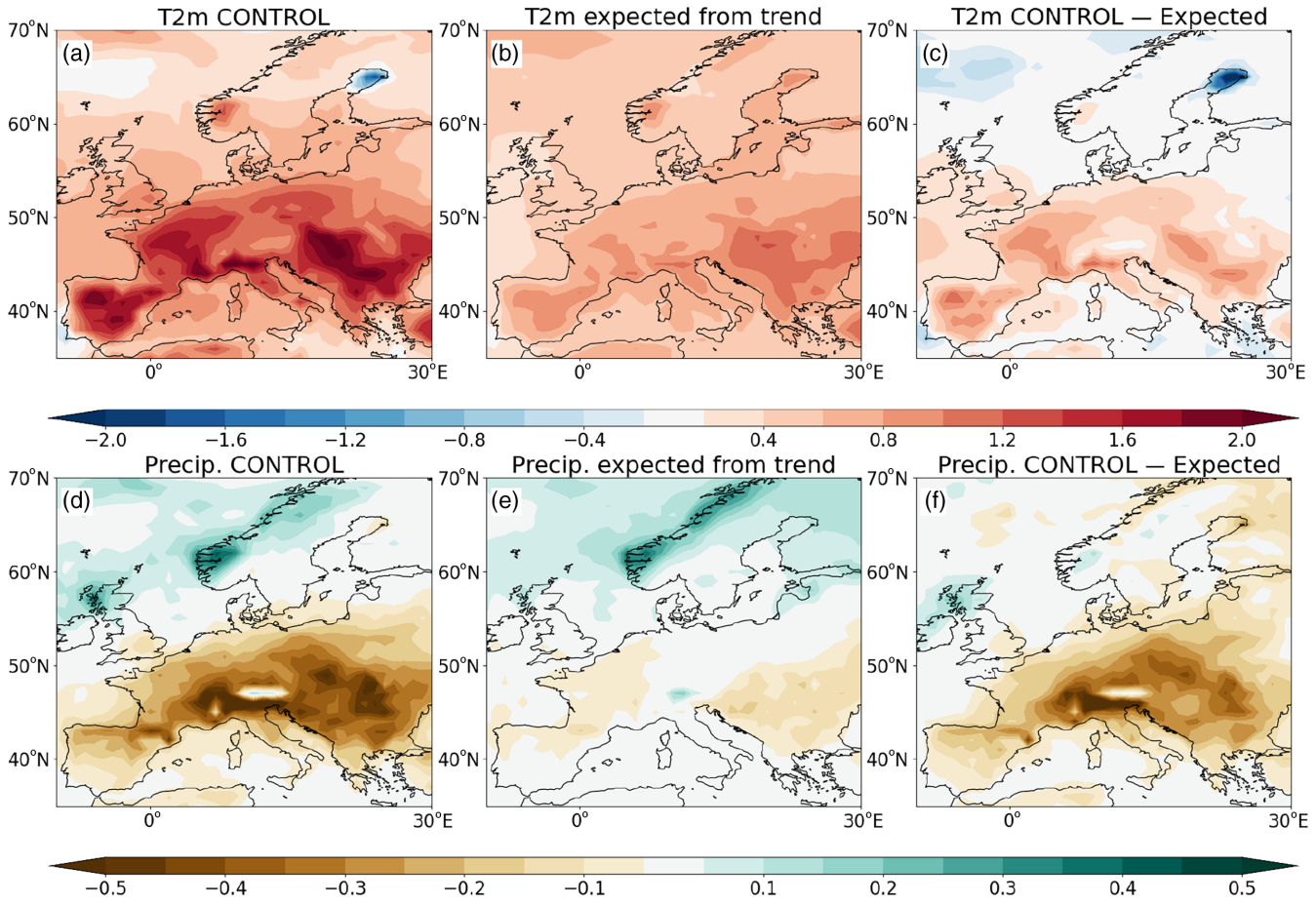


**FIGURE 12** CONTROL June–August (JJA)-mean, ensemble-mean (a) 2-m temperature (T2m) and (c) precipitation anomalies compared with expected anomalies in (b) T2m and (d) precipitation extrapolated from trends in the hindcasts and forecasts (1981–2021). Units are (a, b) K and (c, d) mm·day$^{-1}$. [Colour figure can be viewed at wileyonlinelibrary.com]

secondary role. For example, comparing Figures 10a, 11c, and 12b, soil moisture and atmospheric circulation can each account for about 0.4–0.6 K of the CONTROL T2m anomaly over central Europe (approximately 45°N–50°N, 0°E–20°E), with the trend attributable for 0.6–0.8 K over the same region. Note that although direct radiative forcing is likely the primary factor in the SEAS5 hindcast trends, multidecadal SST variability (whether externally forced or internal ocean variability) may also contribute. Atmospheric circulation can account for the majority of the precipitation, particularly for western Europe, but trends also make a small contribution to the CONTROL anomalies.

## 6 | DISCUSSION AND CONCLUSIONS

This study has analysed drivers of circulation and surface weather in hindcasts and observations of the hot and dry 2022 European summer. In this final section we draw a number of conclusions from this work. First, we return to the questions we asked in Section 1.

- How well did ECMWF's SEAS5 capture the observed circulation and near-surface anomalies in European summer 2022?

In spite of low skill in general for predictions of summertime atmospheric circulation, SEAS5 predictions, initialised on May 1 for JJA 2022 were relatively accurate. We analysed a SEAS5 hindcast of the 2022 summer season with the same set-up as the original real-time forecast, but using 200 members rather than 51. This hindcast is referred to as the CONTROL hindcast. The ensemble-mean predicted a northward-shifted North Atlantic jet and warm and dry anomalies across much of Europe (Figure 2e–g). These predictions matched up well with the observations, although the observed jet shift extended further into Europe (Figure 2c) and the observed dry anomalies were more confined to northwest and central Europe (Figure 2b). The magnitudes of the observed Europe-average T2m and precipitation anomalies also lay

within the model ensemble, albeit at the hot and dry ends of the distributions respectively (Figure 3j,k).

- What determined the circulation patterns in observations and the forecast? Did the forecast capture circulation anomalies for the 'right reasons'?

We investigated the influence of the three predictors: stratospheric vortex strength, Niño 3.4 SSTs, and the linear trend on U500 anomalies using ERA5 data for 1981–2021. A southward jet trend explains a large amount of the U500 interannual variance and dominates the statistical prediction for 2022 over the other two predictors (Figure 5c,d), which both tend to shift the jet northward (Figure 5a,b). Overall, this statistical model explains little of the historical U500 variability (Figure 5f), and it appears that the circulation was not predictable based on these drivers alone. This does not preclude the possibility of other drivers contributing to the observed jet shift. Further work could examine the extent to which the observed circulation was driven by unpredictable noise versus predictable signal via a linear-inverse method such as Albers *et al.* (2022).

A similar statistical model applied to the CONTROL, using SEAS5 hindcasts and forecasts for 1981–2021 and the same three drivers, overall suggests a northward-shifted jet, similar to that seen for the full model prediction (Figure 6e,f). Though the stratospheric vortex strength and Niño 3.4 SSTs both contribute to the circulation anomalies (Figure 6a,b), a large part of this prediction comes from a northward jet trend in the model (Figure 6c). This northward jet trend contrasts with the observed southward shift over recent decades (Figure 5c).

To investigate the role of different aspects of the initial conditions in driving the CONTROL circulation, additional hindcast experiments were performed with only 2022 ocean initial conditions (OCEAN-IC-2022) and with only 2022 atmospheric and land-surface conditions (ATMOS-IC-2022). These experiments show that ocean initial conditions dominate the CONTROL circulation anomalies (Figure 7). This also suggests that the model jet trend is driven by trends in SSTs rather than by direct radiative forcing. These SST trends may in turn be driven by radiative forcing or be related to long time-scale internal ocean variability. Further work is required to attribute the drivers of summer circulation trends in the model and observations and assess the relative roles of external forcing and internal variability.

- What role did the atmospheric circulation, externally forced trends, and soil moisture anomalies play in driving the forecast near-surface conditions?

Although the CONTROL atmospheric circulation anomalies are dominated by ocean initial conditions, other aspects of the initial state contribute strongly to the T2m and precipitation anomalies (Figure 8b,e). The majority of the CONTROL T2m anomalies are reproduced in the ATMOS-IC-2022 experiment (Figure 8a,b). The ATMOS-IC-2022 T2m anomalies are likely driven by radiative forcing from higher greenhouse gas levels relative to the climatology period and by a reduction in latent cooling due to dry initial soil moisture anomalies (Figure 11c). A circulation analogues analysis suggests that atmospheric circulation makes a secondary contribution, with the largest effect of circulation on T2m being in south-west Europe (Figure 10a,c). Conversely, atmospheric circulation appears to be a large factor driving precipitation anomalies in the CONTROL, particularly in western Europe (Figure 10d,j).

This case study demonstrates that at least some aspects of European summers, such as T2m, are predictable at 2- to 4-month lead times due to long-term radiative forcing trends and the land-surface initial state. In the case of the European summer 2022, the SEAS5 atmospheric circulation prediction was consistent with a long-term northward trend in the model as well as negative Niño 3.4 anomalies and positive stratospheric vortex anomalies. However, analysis of past summer circulation variability suggests that these factors explain only a small proportion of North Atlantic circulation, in general.

It is striking that such a large proportion of the model circulation signal is determined by the long-term trend, though this may point to the relatively weak signals from other sources compared with winter. The discrepancy between the modelled northward jet trend and the observed southward shift merits further investigation as it could be a source of forecast error. This would involve understanding the degree to which the observed trend is driven by internal variability and whether the model can capture such internal variability. It would also be of interest to investigate whether strong circulation trends exist in other seasonal forecast systems. Dong and Sutton (2021) argue that aerosol trends may be a cause of the observed summer jet changes. Hence, it is possible that implementing a more comprehensive representation of aerosol interactions in future forecast systems could alleviate this trend difference. In the interim, it may be useful to investigate post-processing of summer forecasts to account for the erroneous trend and incorporate the effects of the actual, southward trend. This approach would, however, only be advisable once drivers of the observed trend are better understood.

Although, the summer 2022 Euro-Atlantic circulation was not as predictable as it first may have appeared, this does not preclude the possibility of predictable windows of opportunity (Dunstone *et al.*, 2023a). For example, this may occur in a year with particularly large stratospheric

vortex or tropical Pacific SST anomalies. One limitation of the linear regression analysis performed in this article is its inability to predict windows of opportunity, so in reality some years may be more predictable than such an analysis would suggest. It is also possible that 2022 European T2m may have been more predictable than usual as hot summers are more predictable than average summers (Wulff & Domeisen, 2019). For these reasons, case studies of well-predicted years can provide a valuable perspective on the potential for predictability in the European summer season.

## ACKNOWLEDGEMENTS

We thank ECMWF for the use of supercomputing resources through a Special Project to run the hindcast experiments described in this study. Finally, we thank two anonymous reviewers for their valuable comments that helped to improve the clarity and robustness of this article.

## CONFLICT OF INTEREST STATEMENT

The authors declare no conflict of interest.

## FUNDING INFORMATION

MP was funded through the NERC-funded project WISHBONE (Grant NE/T013451/1). COR was supported by a Royal Society University Research Fellowship. AW received funding from the European Union's Horizon Europe research and innovation programme under Grant agreement no. 101081460 and from UKRI NERC (Grant NE/V001787/1).

## DATA AVAILABILITY STATEMENT

ERA5 and SEAS5/C3S hindcast data were obtained from the Climate Data Store website, https://cds.climate.copernicus.eu. GPCP data were obtained from https://psl.noaa.gov/data/gridded/data.gpcp.html. Data from the experiments performed for this study can be accessed on the CEDA website at https://catalogue.ceda.ac.uk/uuid/235e3307338c4168816871a314eada4f.

## ORCID

*Matthew Patterson* https://orcid.org/0000-0002-9484-8410
*Christopher H. O'Reilly* https://orcid.org/0000-0002-8630-1650
*Antje Weisheimer* https://orcid.org/0000-0002-7231-6974

## REFERENCES

Adler, R.F., Sapiano, M., Huffman, G.J., Wang, J., Gu, G., Bolvin, D. et al. (2018) The global precipitation climatology project (GPCP) monthly analysis (new version 2.3) and a review of 2017 global precipitation. *Atmosphere*, 9, 138.

Albers, J.R., Newman, M., Hoell, A., Breeden, M.L., Wang, Y. & Lou, J. (2022) The February 2021 cold air outbreak in the United States: a subseasonal forecast of opportunity. *Bulletin of the American Meteorological Society*, 103, E2887–E2904. Available from: https://journals.ametsoc.org/view/journals/bams/103/12/BAMS-D-21-0266.1.xml

Ardilouze, C., Batté, L., Bunzel, F., Decremer, D., Déqué, M., Doblas-Reyes, F.J. et al. (2017) Multi-model assessment of the impact of soil moisture initialization on mid-latitude summer predictability. *Climate Dynamics*, 49, 3959–3974. Available from: https://doi.org/10.1007/s00382-017-3555-7

Athanasiadis, P.J., Bellucci, A., Scaife, A.A., Hermanson, L., Materia, S., Sanna, A. et al. (2017) A multisystem view of wintertime NAO seasonal predictions. *Journal of Climate*, 30, 1461–1475. Available from: https://journals.ametsoc.org/view/journals/clim/30/4/jcli-d-16-0153.1.xml

Ballester, J., Quijal-Zamorano, M., Méndez Turrubiates, R.F., Pegenaute, F., Herrmann, F.R., Robine, J.M. et al. (2023) Heat-related mortality in Europe during the summer of 2022. *Nature Medicine*, 29, 1857–1866. Available from: https://www.nature.com/articles/s41591-023-02419-z

Beobide-Arsuaga, G., Düsterhus, A., Müller, W.A., Barnes, E.A. & Baehr, J. (2023) Spring regional sea surface temperatures as a precursor of European summer heatwaves. *Geophysical Research Letters*, 50, e2022GL100727. Available from: https://doi.org/10.1029/2022GL100727

Bonaldo, D., Bellafiore, D., Ferrarin, C., Ferretti, R., Ricchi, A., Sangelantoni, L. et al. (2022) The summer 2022 drought: a taste of future climate for the Po valley (Italy)? *Regional Environmental Change*, 23, 1. Available from: https://doi.org/10.1007/s10113-022-02004-z

Christidis, N., Jones, G.S. & Stott, P.A. (2015) Dramatically increasing chance of extremely hot summers since the 2003 European heatwave. *Nature Climate Change*, 5, 46–50. Available from: https://www.nature.com/articles/nclimate2468

Copernicus. (2022) *European state of the climate summary*. Technical Report. https://climate.copernicus.eu/sites/default/files/custom-uploads/ESOTC2022/PR/ESOTCsummary2022_final.pdf

Domeisen, D.I.V., Butler, A.H., Fröhlich, K., Bittner, M., Müller, W.A. & Baehr, J. (2015, 271) Seasonal predictability over Europe arising from El Niño and stratospheric variability in the MPI-ESM seasonal prediction system. *Journal of Climate*, 28, 256. Available from: https://journals.ametsoc.org/view/journals/clim/28/1/jcli-d-14-00207.1.xml

Dong, B. & Sutton, R.T. (2021) Recent trends in summer atmospheric circulation in the North Atlantic/European region: is there a role for anthropogenic aerosols? *Journal of Climate*, 34, 6777–6795. Available from: https://journals.ametsoc.org/view/journals/clim/34/16/JCLI-D-20-0665.1.xml

Dunstone, N., Smith, D., Hardiman, S., Eade, R., Gordon, M., Hermanson, L. et al. (2019) Skilful real-time seasonal forecasts of the dry northern European summer 2018. *Geophysical Research Letters*, 46, 12368–12376. Available from: https://doi.org/10.1029/2019GL084659

Dunstone, N., Smith, D., Scaife, A., Hermanson, L., Fereday, D., O'Reilly, C. et al. (2018) Skilful seasonal predictions of summer European rainfall. *Geophysical Research Letters*, 45, 3246–3254. Available from: https://doi.org/10.1002/2017GL076337

Dunstone, N., Smith, D.M., Hardiman, S.C., Davies, P., Ineson, S., Jain, S. et al. (2023a) Windows of opportunity for predicting

seasonal climate extremes highlighted by the Pakistan floods of 2022. *Nature Communications*, 14, 6544. Available from: https://www.nature.com/articles/s41467-023-42377-1

Dunstone, N., Smith, D.M., Hardiman, S.C., Hermanson, L., Ineson, S., Kay, G. et al. (2023b) Skilful predictions of the summer North Atlantic oscillation. *Communications Earth & Environment*, 4, 1–11. Available from: https://www.nature.com/articles/s43247-023-01063-2

Faranda, D., Pascale, S. & Bulut, B. (2023) Persistent anticyclonic conditions and climate change exacerbated the exceptional 2022 European-Mediterranean drought. *Environmental Research Letters*, 18, 034030. Available from: https://doi.org/10.1088/1748-9326/acbc37

Franzke, C. & Woollings, T. (2011) On the persistence and predictability properties of North Atlantic climate variability. *Journal of Climate*, 24, 466–472. Available from: https://journals.ametsoc.org/view/journals/clim/24/2/2010jcli3739.1.xml

Harvey, B., Hawkins, E. & Sutton, R. (2023) Storylines for future changes of the North Atlantic jet and associated impacts on the UK. *International Journal of Climatology*, 43, 4424–4441. Available from: https://doi.org/10.1002/joc.8095

Hersbach, H., Bell, B., Berrisford, P., Hirahara, S., Horányi, A., Muñoz-Sabater, J. et al. (2020) The ERA5 global reanalysis. *Quarterly Journal of the Royal Meteorological Society*, 146, 1999–2049. Available from: https://doi.org/10.1002/qj.3803

Ibebuchi, C.C. & Abu, I.-O. (2023) Characterization of temperature regimes in Western Europe, as regards the summer 2022 Western European heat wave. *Climate Dynamics*, 61, 3707–3720. Available from: https://doi.org/10.1007/s00382-023-06760-4

Jézéquel, A., Yiou, P. & Radanovics, S. (2018) Role of circulation in European heatwaves using flow analogues. *Climate Dynamics*, 50, 1145–1159. Available from: https://doi.org/10.1007/s00382-017-3667-0

Johnson, S.J., Stockdale, T.N., Ferranti, L., Balmaseda, M.A., Molteni, F., Magnusson, L. et al. (2019) SEAS5: the new ECMWF seasonal forecast system. *Geoscientific Model Development*, 12, 1087–1117. Available from: https://gmd.copernicus.org/articles/12/1087/2019/

Lockwood, J.F., Stringer, N., Hodge, K.R., Bett, P.E., Knight, J., Smith, D. et al. (2023) Seasonal prediction of UK mean and extreme winds. *Quarterly Journal of the Royal Meteorological Society*, 149, 3477–3489. Available from: https://doi.org/10.1002/qj.4568

O'Reilly, C.H., Woollings, T., Zanna, L. & Weisheimer, A. (2018) The impact of tropical precipitation on summertime Euro-Atlantic circulation via a circumglobal wave train. *Journal of Climate*, 31, 6481–6504. Available from: https://journals.ametsoc.org/view/journals/clim/31/16/jcli-d-17-0451.1.xml

Orth, R. & Seneviratne, S.I. (2014) Using soil moisture forecasts for sub-seasonal summer temperature predictions in Europe. *Climate Dynamics*, 43, 3403–3418. Available from: https://doi.org/10.1007/s00382-014-2112-x

Osborne, J.M., Collins, M., Screen, J.A., Thomson, S.I. & Dunstone, N. (2020) The North Atlantic as a driver of summer atmospheric circulation. *Journal of Climate*, 33, 7335–7351. Available from: https://journals.ametsoc.org/view/journals/clim/33/17/jcliD190423.xml

Ossó, A., Sutton, R., Shaffrey, L. & Dong, B. (2018) Observational evidence of European summer weather patterns predictable from spring. *Proceedings of the National Academy of Sciences*, 115, 59–63. Available from: https://doi.org/10.1073/pnas.1713146114

Ossó, A., Sutton, R., Shaffrey, L. & Dong, B. (2020) Development, amplification, and decay of Atlantic/European summer weather patterns linked to spring North Atlantic Sea surface temperatures. *Journal of Climate*, 33, 5939–5951. Available from: https://journals.ametsoc.org/view/journals/clim/33/14/JCLI-D-19-0613.1.xml

Patterson, M. (2023) North-West Europe hottest days are warming twice as fast as mean summer days. *Geophysical Research Letters*, 50, e2023GL102757. Available from: https://doi.org/10.1029/2023GL102757

Patterson, M., Weisheimer, A., Befort, D.J. & O'Reilly, C. (2022) The strong role of external forcing in seasonal forecasts of European summer temperature. *Environmental Research Letters*, 17, 104033. Available from: https://doi.org/10.1088/1748-9326/ac9243

Perkins-Kirkpatrick, S.E. & Lewis, S.C. (2020) Increasing trends in regional heatwaves. *Nature Communications*, 11, 3357. Available from: https://www.nature.com/articles/s41467-020-16970-7

Prodhomme, C., Doblas-Reyes, F., Bellprat, O. & Dutra, E. (2016) Impact of land-surface initialization on sub-seasonal to seasonal forecasts over Europe. *Climate Dynamics*, 47, 919–935. Available from: https://doi.org/10.1007/s00382-015-2879-4

Rieke, O., Greatbatch, R.J. & Gollan, G. (2021) Nonstationarity of the link between the tropics and the summer East Atlantic pattern. *Atmospheric Science Letters*, 22, e1026. Available from: https://doi.org/10.1002/asl.1026

Rodrigues, M., Camprubí, À.C., Balaguer-Romano, R., Coco Megía, C.J., Castañares, F., Ruffault, J. et al. (2023) Drivers and implications of the extreme 2022 wildfire season in Southwest Europe. *Science of the Total Environment*, 859, 160320. Available from: https://www.sciencedirect.com/science/article/pii/S0048969722074204

Rousi, E., Kornhuber, K., Beobide-Arsuaga, G., Luo, F. & Coumou, D. (2022) Accelerated western European heatwave trends linked to more-persistent double jets over Eurasia. *Nature Communications*, 13, 3851. Available from: https://www.nature.com/articles/s41467-022-31432-y

Scaife, A.A., Arribas, A., Blockley, E., Brookshaw, A., Clark, R.T., Dunstone, N. et al. (2014) Skillful long-range prediction of European and North American winters. *Geophysical Research Letters*, 41, 2514–2519. Available from: https://doi.org/10.1002/2014GL059637

Schumacher, D.L., Zachariah, M. & Otto, F. (2022) *High temperatures exacerbated by climate change made 2022 northern hemisphere droughts more likely*. London: World Weather Attribution (WWA). Available from: https://policycommons.net/artifacts/3174587/wce-nh-drought-scientific-report/3973082/

Seneviratne, S.I., Corti, T., Davin, E.L., Hirschi, M., Jaeger, E.B., Lehner, I. et al. (2010) Investigating soil moisture–climate interactions in a changing climate: a review. *Earth-Science Reviews*, 99, 125–161. Available from: https://www.sciencedirect.com/science/article/pii/S0012825210000139

Wang, L. & Ting, M. (2022) Stratosphere-troposphere coupling leading to extended seasonal predictability of summer North Atlantic oscillation and boreal climate. *Geophysical Research Letters*, 49, e2021GL096362. Available from: https://doi.org/10.1029/2021GL096362

Wulff, C.O. & Domeisen, D.I.V. (2019) Higher subseasonal predictability of extreme hot European summer temperatures as compared to average summers. *Geophysical Research Letters*,

46, 11520–11529. Available from: https://doi.org/10.1029/2019GL084314

Wulff, C.O., Greatbatch, R.J., Domeisen, D.I.V., Gollan, G. & Hansen, F. (2017) Tropical forcing of the summer East Atlantic pattern. *Geophysical Research Letters*, 44, 11166–11173. Available from: https://doi.org/10.1002/2017GL075493

Zachariah, M., Vautard, R., Schumacher, D.L., Vahlberg, M., Heinrich, D., Raju, E. et al. (2022) Without human-caused climate change temperatures of 40°C in the UK would have been extremely unlikely. p. 26.

Zuo, H., Balmaseda, M.A., Tietsche, S., Mogensen, K. & Mayer, M. (2019) The ECMWF operational ensemble reanalysis–analysis system for ocean and sea ice: a description of the system and assessment. *Ocean Science*, 15, 779–808. Available from: https://os.copernicus.org/articles/15/779/2019/

## SUPPORTING INFORMATION

Additional supporting information can be found online in the Supporting Information section at the end of this article.

**How to cite this article:** Patterson, M., Befort, D.J., O'Reilly, C.H. & Weisheimer, A. (2024) Drivers of the ECMWF SEAS5 seasonal forecast for the hot and dry European summer of 2022. *Quarterly Journal of the Royal Meteorological Society*, 1–18. Available from: https://doi.org/10.1002/qj.4851